HEAT TRANSFER BY SEEPAGE IN SAND: INFLUENCE OF SATURATED HYDRAULIC CONDUCTIVITY AND POROSITY

VPLIV KOEFICIENTA PREPUSTNOSTI IN POROZNOSTI ZEMLJIN NA PRENOS TOPLOTE S PRECEJANJEM

Yaser Ghafoori[1,*1], Matej Maček[1], Andrej Vidmar[1], Jaromír Říha[2], Andrej Kryžanowski[1]

[1] Faculty of Civil and Geodetic Engineering, University of Ljubljana, Jamova cesta 2, 1000 Ljubljana, Slovenia

[2] Faculty of Civil Engineering, Brno University of Technology, Veveří 331/95, 602 00 Brno, Czech Republic

Abstract

Heat transfer within the soil is a complex process in the presence of seepage flow. In such conditions, the soil's thermal behavior is influenced by the thermal and hydraulic properties of the medium as well as the initial conditions and boundary conditions to which the medium is subjected. This paper presents the experimental and numerical studies of heat transfer within the sand subjected to the seepage flow. It focuses on the influence of saturated hydraulic conductivity and the porosity of medium on the heat transfer process. The temperature distribution within the sand was monitored by the optical fiber Distributed Temperature Sensor (DTS). The experiment was performed on three types of silica-dominated sands with different saturated hydraulic conductivities and different Soil Water Characteristic Curve (SWCC). In addition to the experimental study, a coupled hydrothermal numerical model was designed in FEFLOW software and validated by comparing its results with the experimental measurements. To determine the influence of porosity and saturated hydraulic conductivity on heat transfer, we analyzed the numerical models for different values of porosity and saturated hydraulic conductivity. The numerical and experimental studies showed that the thermal velocity is higher in sand with higher saturated hydraulic conductivity and temperature declination occurs more quickly due to the heat convection process. Saturated sand with larger porosity has an overall higher heat capacity, wherefore the temperature declination started later in the measuring points but dropped down lower close to the temperature of the upstream water.

Izvleček

Prenos toplote s precejanjem v zemljinah predstavlja kompleksen problem. Na termično stanje zemljin vplivajo različni dejavniki, kot so toplotne in hidravlične lastnosti zemljin kot tudi njihova izpostavljenost obratovalnim pogojem ter omejitvam, ki jih narekujejo robni pogoji. V prispevku so predstavljeni rezultati

---

* Stik / *Correspondence*: yaser.ghafoori@fgg.uni-lj.si

raziskav prenosa toplote s precejanjem vode v zemljinah na podlagi primerjave laboratorijskih raziskav in računskega modela. Raziskavo smo usmerili v preučevanje vpliva koeficienta prepustnosti in poroznosti zemljine na proces prenosa toplote. Spremembe temperaturnega polja v eksperimentalni posodi smo merili z optičnimi kabli. Meritve temperaturnega polja v eksperimentalni posodi smo izvajali na treh različnih vzorcih kremenčevega peska s spreminjanjem stopnje poroznosti in koeficienta prepustnosti zemljine. Poleg eksperimentalnega dela smo zasnovali hidravlično-toplotni numerični model v programskem okolju FEFLOW za potrebe primerjalne analize merjenih in računskih vrednosti. Za ugotavljanje vpliva poroznosti in koeficienta prepustnosti v nasičeni zemljini na prenos toplote smo analizirali numerične modele za različne vrednosti teh dveh parametrov. Rezultati laboratorijskih preiskav in numeričnega modela so pokazali, da je hitrost prenosa toplote v materialih z večjim koeficientom prepustnosti večja, posledično je hitrejši upad temperature zaradi konvekcije. V bolj poroznih materialih je upad temperature zaznan kasneje, a je bolj izrazit in se približa vrednostim temperature okoliškega vodnega medija.

Ključne besede: Prenos toplote, poroznost, koeficient prepustnosti, temperature, precejanje.

1. Introduction

The temperature distribution within the earthfill dams is monitored to trace the seepage flow. Although the temperature data do not provide any direct information about the seepage, several methods have been developed to interpret temperature measurements for seepage detection (Dornstädter and Heinemann, 2012; Mars et al., 2013; Sjödahl et al., 2009). One proposed method for seepage detection is to compare the measured temperature within the structure with the simulated numerical results (Ghafoori et al., 2020c). To simulate the heat transfer in the soil, numerical modeling based on the coupled hydrothermal analysis is required. Results of the analysis are dependent on the model's characteristics (e.g. model size and its temporal and spatial discretization), material properties, and initial and boundary conditions. A coupled hydrothermal analysis requires the soil's thermal and hydraulic properties to be determined. While the experimental tests exist for the determination of these parameters, different empirical approaches can also be used to estimate their quantity. The soil's thermal properties, including the volumetric heat capacity and thermal conductivity, should be determined. Additionally, the soil porosity and heat dispersivity also affect the heat transfer process. For the transient analysis, the hydraulic properties of soil should be determined both in saturated and unsaturated conditions.

The current study focuses on the influences of saturated hydraulic conductivity and porosity on the heat transfer by seepage in soil that is initially in an unsaturated condition. It is important to determine this effect, especially for hydraulic conductivity, because the determination of hydraulic conductivity from the laboratory measurement and the estimation methods is subjected to inaccuracies based on the type of materials and the employed method (Hala et al., 2020; Nagy et al., 2013).

This article studies heat transfer experimentally within three types of silica sand subjected to seepage flow. Additionally, the influences of porosity and saturated hydraulic conductivity are studied by a coupled hydrothermal numerical model implemented within the FEFLOW software. It was assumed that the sand is homogenously replaced within the model and the effect of the optical fiber on seepage and heat transport was considered negligible. However, for the real structures, anisotropy plays an important role and should be considered in the analysis. The FEFLOW program has been already employed by Bui et al. (2019) in a coupled seepage and heat transfer study within a laboratory model. In this paper, we employed FEFLOW for the numerical simulation of heat transfer by seepage considering the uncertainties and possible errors in the determination of the saturated hydraulic conductivity and porosity of the used sand. Based on the possible instrumental, procedural, and

human errors, different values for both saturated hydraulic conductivity and porosity are used in the numerical modeling to present their influence on the heat transfer process within the sand. The obtained results in this paper show that the variation in these properties has a remarkable effect on the heat transfer process.

2. Heat transfer within the porous media

The heat is transferred in porous media by three mechanisms: conduction, convection, and radiation. For application in seepage monitoring, the effect of radiation can be negligible. In the absence of seepage flow, heat is transferred purely by the conduction process, while in a porous media subjected to the seepage flow, convection also transfers heat. Within a fully saturated medium, conduction occurs by the grain particles and the liquid that occupies the pores. In the variably saturated medium, conduction within the medium's pores is also affected by the presence of air. Thus the conduction process within porous media depends on the structure of the media matrix and the thermal conductivity of each phase (Kaviany, 1991).

Considering the energy balance equation in a Representative Elementary Volume (REV) of soil, heat transfer can be described by two thermal models, the equilibrium and non-equilibrium ones. Here, the thermal equilibrium approach is considered, where a local thermal equilibrium between the phases of porous media is valid; $T_s = T_f = T$. Where, T_s and T_f are the temperature of solid and fluid phases respectively. In this case, the heat transfer between the phases of porous media is neglected. Averaging over the REV of porous media with porosity n, the energy balance equation for each solid and fluid phase can be written as (Nield and Bejan, 2006):

Solid-phase:

$$(1-n)(\rho c)_s \frac{\partial T_s}{\partial t} = (1-n)\nabla \cdot (\lambda_s \nabla T_s) + (1-n)q_s''' \quad (1)$$

Fluid-phase:

$$n(\rho c)_f \frac{\partial T_f}{\partial t} + (\rho c)_f . \mathbf{v} . \nabla T_f = n\nabla \cdot (\lambda_f \nabla T_f) + nq_f''' \quad (2)$$

where, subscripts s and f represent the solid and fluid phases respectively; ρ is the density $[\frac{\text{kg}}{\text{m}^3}]$; T is the temperature [K]; c is the specific heat capacity $[\frac{\text{J}}{\text{kg K}}]$; t is time [s]; λ is the thermal conductivity $[\frac{\text{W}}{\text{m K}}]$; $\mathbf{v}$ is the Darcy velocity of seepage $[\frac{\text{m}}{\text{s}}]$, and q''' is the volumetric heat generation of porous media $[\frac{\text{W}}{\text{m}^3}]$, which can be neglected in most practical applications. A substance's heat capacity can also be expressed by the volumetric heat capacity c_V $[\frac{\text{J}}{\text{m}^3 \text{K}}]$, which is the specific heat capacity times the substance's density.

The second term in Eq. 2 ($(\rho c)_f . \mathbf{v} . \nabla T_f$) presents the rate of change of thermal energy in REV due to the convection process by the seepage flow. When the fluid flow takes place, the heat transfer by convection is far more efficient than the pure conduction (Dornstadter, 1997). Considering the local thermal equilibrium condition, the energy balance equation for overall porous media is obtained by combining Eq. 1 and Eq. 2:

$$(\rho c)_m \frac{\partial T}{\partial t} + (\rho c)_f . \mathbf{v} . \nabla T = \nabla \cdot (\lambda_m \nabla T) + q''' \quad (3)$$

where subscript m represents the overall porous media, including both solid and fluid phases.

For the variably saturated soil, two fluid phases coexist in the pores; gas (typically air) and fluid (typically water). For modeling heat transfer, the effect of gas in pores should be considered in the soil's thermal properties. The thermal properties of soil depend on its degree of saturation. Considering the double fluid phases (air and water), the equivalent heat capacity and thermal conductivity of the soil can be estimated by Eq. 4 and Eq. 5 respectively (Brinkgreve et al., 2017).

$$(\rho c)_m = (1-n)(\rho c)_s + ns(\rho c)_f + n(1-s)(\rho c)_g \quad (4)$$

$$\lambda_m = (1-n)\lambda_s + ns\lambda_f + n(1-s)\lambda_g \quad (5)$$

where s is the degree of saturation and $(\rho c)_g$ and λ_g are the volumetric heat capacity and thermal conductivity of gas respectively.

Eq. 4 and Eq. 5 can be simplified for the saturated porous media by neglecting the effect of air,

considering the degree of saturation of soil equals 1.

The simplified Eq. 3 for the local thermal equilibrium also fails to consider the effect of the thermal dispersion of the soil. The dispersion effect can be added to Eq. 3 by inserting the heat dispersion tensor ($\boldsymbol{d}$) (which is transformed into the Cartesian coordinate) into the right side of the equation (Liu and Masliyah, 2005; Rubin, 1974).

$$(\rho c)_m \frac{\partial T}{\partial t} + (\rho c)_f . \mathbf{v}. \nabla T = \nabla \cdot (\lambda_m \nabla T) + n(\rho c)_f (\boldsymbol{d}. \nabla T) \tag{6}$$

Eq. 6 can be written in a different form by introducing the total thermal diffusivity tensor ($\boldsymbol{D}$):

$$(\rho c)_m \frac{\partial T}{\partial t} + (\rho c)_f . \mathbf{v}. \nabla T = (\rho c)_f \nabla \cdot (\boldsymbol{D}. \nabla T) \tag{7}$$

where

$$\boldsymbol{D} = \frac{\lambda_m}{(\rho c)_f} + n\boldsymbol{d}, \tag{8}$$

and λ_m is the thermal conductivity tensor of the medium.

The heat dispersion in the porous media is a function of flow velocity, the medium structure, porosity, the ratio of thermal conductivities, and the ratio of volumetric heat capacities of solid and fluid phases (Kaviany, 1991). Within an isothermal medium, the heat dispersion tensor corresponding to the local coordinates is a diagonal matrix with non-zero components that can be expressed by the longitudinal and transverse dispersion coefficients (Diersch, 2014). At any point of medium, one principle direction of dispersion tensor is along the main flow direction at that point and two other directions are perpendicular to the main flow direction. The dispersion tensor can be transformed to the Cartesian coordinate using Eq. 8 (Bear and Verruijt, 1987; Diersch, 2014).

$$\boldsymbol{d}_{ij} = \beta_t |\mathbf{v}| \delta_{ij} + (\beta_l - \beta_t) \frac{\mathbf{v} \otimes \mathbf{v}}{|\mathbf{v}|} \tag{9}$$

where β_l and β_t are the longitudinal and transverse dispersivity of soil respectively, and δ_{ij} is the Kronecker delta.

In a simple, one-direction flow and when the main flow is along the x-axis, the heat dispersion coefficient can be simplified as Eq. 9 (Mohseni Languri and Domairrry Ganji, 2011).

$$\boldsymbol{d} = \begin{vmatrix} \beta_l |\mathbf{v}| & 0 & 0 \\ 0 & \beta_t |\mathbf{v}| & 0 \\ 0 & 0 & \beta_t |\mathbf{v}| \end{vmatrix} \tag{10}$$

3. Method

3.1 Material

Three types of silica-dominated sand, namely MP1, MP2, and MP3, with different grain size distribution and saturated hydraulic conductivities, were used in this study. MP1 and MP3 sand were purchased in 2019 from TERMIT d.d., a mining company located in Moravče, Slovenia. MP2 sand was purchased in 2019 from KEMA d.o.o, a producer of sand and construction materials located in Puconci, Slovenia. The mineralogical compositions of the sand were provided by the vendors (Kema, 2020; Termit, 2018) and are shown in Table 1.

Table 1: Mineralogical composition of sand.

Preglednica 1: Mineraloška sestava vzorcev peska.

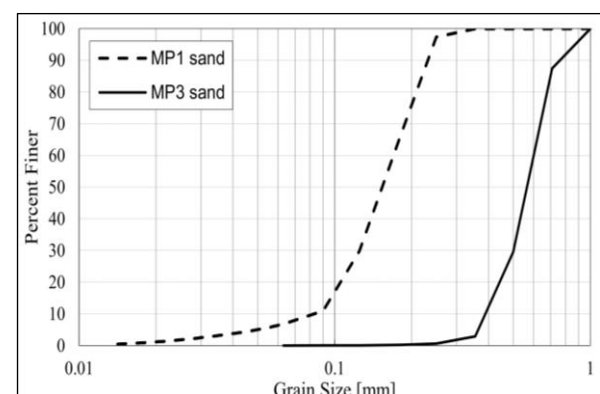| Mineralogical composition				
SiO$_2$ %	Fe$_2$O$_3$ %	Al$_2$O$_3$ %	TiO$_2$ %	K$_2$O %
MP1 & MP3 sand				
99.17	0.12	0.35	0.07	0.10
MP2 sand				
> 98.00	0.30	0.66	0.03	0.10

Figure 1: *Grain size distribution of MP1 and MP3 sand.*

Slika 1: *Granulometrični krivulji za vzorca MP1 in MP3.*

For MP1 and MP3 sand, the grain size distribution curves were determined by the sieve analysis as shown in Figure 1.

The sand's porosity was calculated from its dry density and particle density. The dry density of each sand was measured in the laboratory tests. The saturated hydraulic conductivity k_{sat} for all three types of sand was measured in the constant head rigid wall permeameter using local total head measurements. The measured saturated hydraulic conductivities of materials are presented in Table 2.

Table 2: *Saturated hydraulic conductivity of materials.*

Preglednica 2: *Koeficient prepustnosti v nasičenih pogojih za preiskane materiale.*

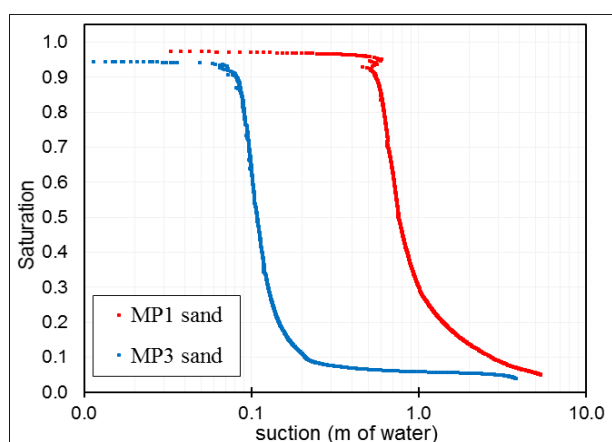| k_{sat} [m/s]		
MP1	MP2	MP3
$1.43 \ 10^{-4}$	$1.50 \ 10^{-3}$	$1.23 \ 10^{-3}$

Figure 2: *The measured SWCC for MP1 and MP3 sand.*

Slika 2: *Retencijska krivulja za vzorca MP1 in MP3.*

The Soil Water Characteristic Curve (SWCC) and the relative hydraulic conductivity curve for MP1 and MP3 sand were determined by the HYPROP device test (Ghafoori et al., 2020a; Schindler and Müller, 2017). The sand in the permeameter and the SWCC mold was compacted to the same dry density as in the experimental model to ensure a better match of hydraulic conductivity in the experiment with the measured value. Figure 2

presents the SWCC for both MP1 and MP3 sand measured in the HYPROP device.

3.2 Experimental study

The experimental model was constructed from Plexiglas and consisted of a small box filled with sand, an upstream tank with an inflow gauge, and a downstream tank with outflow. The sand box was supported and separated from the upstream and downstream tanks by wire meshes. The sand was compacted by a hand tamper in the experimental model. The same experiment was repeated for all three types of silica sand. A passive optical fiber DTS system with a spatial resolution equals 0.63 m was employed for temperature measurement within the sand. The XT-DTS system which is manufactured by Silixa Ltd measures the temperature with an accuracy as high as 0.1 °C for 5 km cable length (Silixa Ltd, 2014). The cable was placed horizontally on three different layers (bottom, middle, and top layers) for the experiments on the MP1 and MP3 sand, and in two different layers (bottom and top layers) for MP2 sand. We formed four measuring points on each layer, two at the sand model's upstream and two at its downstream. Each pair of measuring points were located symmetrically with respect to the model vertical central plane as shown in Figure 3d. The distribution of the cable in the three sets of the experiment is shown in Figure 3. The width of the sand-fill was 27 cm for all three sets of the experiment. In Figure 3, UP represents the measuring points located near the upstream side of the model and DOWN indicates the points located near the downstream side of the model. In each elevation, two points were formed near the upstream and two near the downstream, which are indicated by the numbers (see Fig 3d). Figures accord with the steady-state and when the water reached the highest recorded level during the experiment.
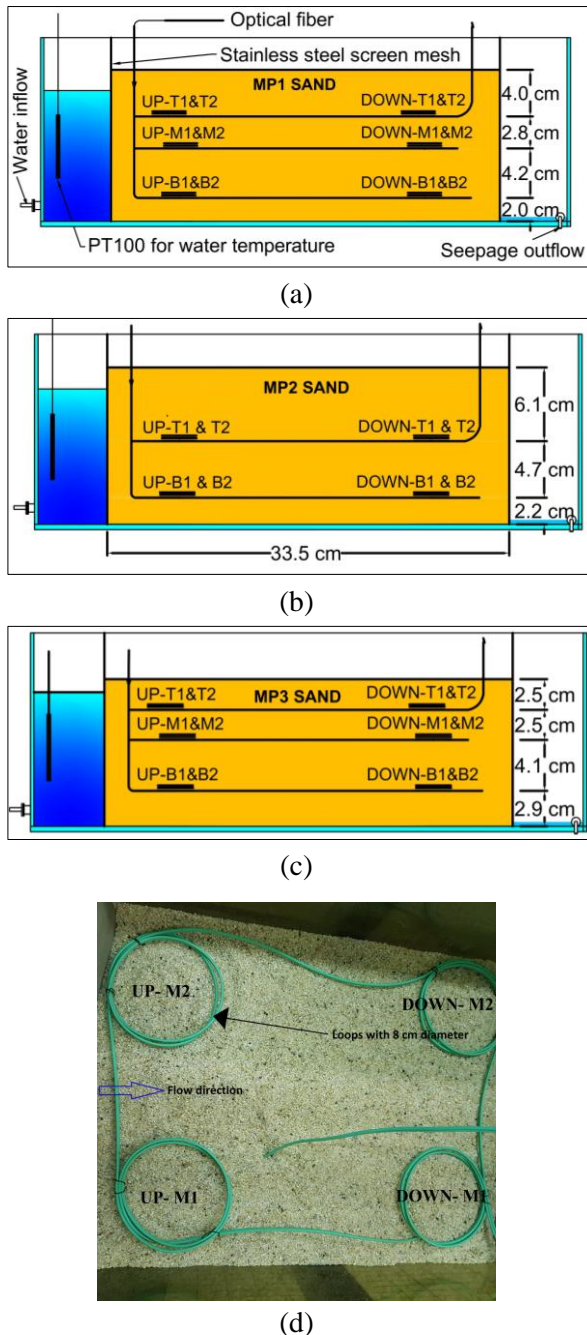
(a)

(b)

(c)

(d)

Figure 3: *Distribution of the cable and the measuring points within the experimental models. (a) MP1 sand (Ghafoori et al., 2020b); (b) MP2 sand (Ghafoori et al., 2020b); (c) MP3 sand (Ghafoori et al., 2020a); and (d) Placement of the cable on the middle layer (Top view).*

Slika 3: *Položaj optičnih kablov in merskih točk v preskusnem modelu; (a) pesek MP1 (Ghafoori et al., 2020b), (b) pesek MP2 (Ghafoori et al., 2020b), (c) pesek MP3* (Ghafoori et al., 2020a) *in (d) položaj kabla na sredini vzorca (pogled od zgoraj).*

The experiment was started by opening the tap water and let the water flows freely from the upstream tank into the sand while the water level at the upstream and downstream was measured at certain time intervals. The temperature of water within the tank was measured continuously by a PT100 thermometer with an accuracy of 0.1 °C attached to the DTS system. The average temperature of water in the upstream tank was 20.5 °C for the experiment with MP1 sand, 19.5 °C for the MP2 sand experiment, and 19.8 °C for the experiment with MP3 sand. In the downstream, the opened outflow gauge allows a free outflow of seepage from the tank.

3.3 Numerical study

The numerical modeling was conducted only on the MP3 sand using the coupled hydrothermal analysis in the FEFLOW (version 7.2) program. We simulated the experimental model in two dimensions coordinate considering a vertical planner projection of the sand box. The simulation for the seepage flow was conducted by the Richards equation for the unsaturated and variably saturated medium, while the transient state was assigned for both flow and heat transport. The sand-fill within the model is assumed to be homogenous. The material's thermal and hydraulic properties, the geometry of the experimental model, and the initial and boundary conditions of the experimental model were considered. The same experiment was also modeled numerically using the geotechnical program PLAXIS 2D by Ghafoori et al. (2020a); however, here, the FEFLOW program was used with different values for the soil's porosity and saturated hydraulic conductivity to determine their influences on the heat transfer. Table 4 presents the material properties of MP3 sand and the method from which these values are obtained.

The saturated hydraulic conductivity was measured in constant head permeameter without saturation control and the porosity was calculated from the laboratory measurement of dry density and particle density (2.7 g/cm³). The determination of both saturated hydraulic conductivity and porosity in the laboratory

measurement can be subject to instrumental, procedural, and human errors. In the case of porosity, the uncertainties are the result of errors in measurements of dry mass, soil volume, particle density, and quality of drying. We estimate the error in porosity to be about 5%. For larger scales and in real size, porosity can be measured with an accuracy as high as ± 0.01. In the measurements of saturated hydraulic conductivity, the uncertainties are mostly due to the effect of dry density, achieved the degree of saturation, homogeneity of the soil matrix, and grain size distribution. The estimated error in the determination of saturated hydraulic conductivity is much greater.

In this paper, we analyzed 6 numerical models for different values of saturated hydraulic conductivity (k_{sat}) within the range of ±10 percent of its measured value and the porosity (n) within the range of ±5 percent of its measured value as shown in Table 3.

Table 3: *The input values for saturated hydraulic conductivity and porosity in numerical modeling.*

Preglednica 3: *Vrednosti koeficienta prepustnosti in poroznosti, ki so uporabljene v numeričnem modelu.*

Numerical models	k_{sat} [m/s]	n
M1 (Measured values)	$1.23 \ 10^{-3}$	0.435
M2 (-10% error in k_{sat})	$1.1 \ 10^{-3}$	0.435
M3 (+10% error in k_{sat})	$1.35 \ 10^{-3}$	0.435
M4 (-5% error in n)	$1.23 \ 10^{-3}$	0.41
M5 (+2.5% error in *n*)	$1.23 \ 10^{-3}$	0.445
M6 (+5% error in *n*)	$1.23 \ 10^{-3}$	0.46

Any change in the value of porosity will affect the hydraulic conductivity; however, both saturated and relatively saturated conductivities were measured independently in separate laboratory tests. Therefore, for each model, the other material properties remain the same as presented in Table 4.

The measured SWCC and the relative hydraulic conductivity curve were modeled by the program using the Van Genuchten equation (Van Genuchten, 1980). The model fitting parameters are presented in Table 4.

The numerical modeling was designed on a vertical two-dimensional (2D) plane, while a transient state analysis was considered based on Richards' equation for the unsaturated and variably saturated medium. The analysis also included the transient state of heat transfer within the soil.

The initial and boundary conditions of the model were defined according to the experimental model. Initially, the sand was at residual saturation with a constant temperature equal to the average measured temperature before the seepage flow (23 ᵒC). Three types of boundary conditions were employed to assign the flow boundary condition of the model. For the upstream face (left boundary), the time-dependent hydraulic head associated with the measured water level at the upstream tank was assigned. For the boundaries at the top and the downstream (right side), the seepage face was considered, while a no-flow boundary (Neumann boundary) was assigned for the bottom of the model. Figure 4 shows the numerical model with its boundary conditions with respect to the flow and the location of the observation point based on the experimental measurement.
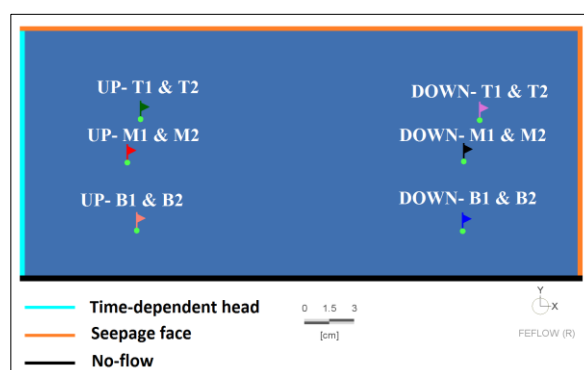

Figure 4: *The flow boundary conditions and the location of observation points within the model.*

Slika 4: *Mejni robni pogoji in lokacija opazovalnih točk na modelu.*

The initial temperature of sand was assumed constant and equals to the average temperature of dry sand. For the thermal boundary, the temperature of the water of 19.8 °C was assigned by the time-dependent function on the upstream face. The bottom of the model, which was the Plexiglas, was considered as an insulation boundary (closed thermal boundary). The upper boundary and the downstream face were exposed to the ambient temperature and the heat is transferred by the heat convection between the boundary and air. This convection is considered negligible relative to the larger heat transfer by the conduction and convection due to seepage propagation. Therefore, these boundaries are also assigned as closed thermal boundaries.

4. Results and discussion

This section presents the temperature distribution results within the sand obtained by the optical fiber DTS measurements and the numerical results by the coupled hydrothermal analysis performed on MP3 sand.

Figure 5 presents the obtained temperature by the optical fiber DTS embedded within the three types of sand at the different times of the experimental study.

The temperature of dry sand (before the experiments) is shown for each sand in curve T = 0 min in Figure 5. The length of the cable associated with the measuring points that are located upstream and downstream of the model is also indicated. The temperature distribution within the three types of sand is strongly based on the difference in their saturated and unsaturated hydraulic behavior. For the MP1 sand, the temperature at the measuring points located near the upstream is dropping fast, because the sand has lower hydraulic conductivity (see Table 2) and the water is moving upward to the free seepage upper boundary due to the capillary rise instead of propagating toward the downstream of the model (see Fig 5a). It can be seen in Figure 5a that the temperature for the points located near the downstream remains almost constant during the

whole experiment and indicates that sand remains dry in this area.

Unlike the MP1 sand, the temperature dropping for the downstream measuring points within the MP2 and MP3 sand is visible in Figures 5b and 5c. They have higher hydraulic conductivity and seepage propagated downstream and exited from the downstream free seepage boundary. The heat is transferred due to the convection by the seepage flow through the sand, and the temperature declination occurred for all measuring points.

Dropping the temperature in a measuring point can be used to calculate the speed of the thermal velocity. Within the seepage zone, convection is the dominant heat transfer process and the thermal velocity is mostly controlled by the heat transfer between the propagated water and the soil. It is clear in Figure 5 that the thermal velocity within the highly permeable MP2 and MP3 sand is higher than the MP1 sand with low hydraulic conductivity. The relation of thermal velocity with the seepage propagation can be used to estimate the seepage velocity within the soil subjected to the seepage flow (Johansson, 1997; Perzlmaier et al., 2007). Bui et al. (2019) used the numerical modeling with FEFLOW, together with the physical modeling of coupled seepage and thermal transportation in soil, to show that temperature measurement is a good parameter for estimating the seepage velocity.

Coupled hydrothermal numerical simulation was conducted for the MP3 sand and the temperature results were validated by the optical fiber DTS measured temperature. Figure 6 presents the temperature variation at 6 measuring points within the MP3 sand measured by optical fiber DTS. The saturation (%) of MP3 sand for time T=12.5 min in Figure 7 shows that all measuring points are almost fully saturated at this time of the experiment.

The influence of saturated hydraulic conductivity also can be described by the temperature results from the numerical modeling of MP3 sand shown in Figure 8. Three different values for the saturated hydraulic conductivity were considered; the value measured in laboratory ($k_{sat} = 1.23 \ 10^{-3}$

m/s), value 10% smaller (k_{sat} = 1.10 10^{-3} m/s), and the value 10% higher than the measured value (k_{sat} = 1.35 10^{-3} m/s). The other parameters and properties remain constant, as in Table 4.

**Table 4:** *Hydraulic and thermal properties of MP3 sand.*

**Preglednica 4:** *Hidravlične in termične lastnosti peska MP3.*

Parameter			Value [unit]	Method of measurement
FLOW	Saturated hydraulic conductivity, k_{sat}		1.23 10^{-3} m/s	Constant head rigid wall permeameter measurement
	Porosity, n		0.435	Calculated from dry density and particle density Measured dry density ρ_d = 1540 [kg/m³]
	Van Genuchten parameters	α_{vg}	9.6 1/m	Laboratory test by HYPROP device and then fit the measurements to the Van Gnuthen model (Van Genuchten, 1980)
		n_{vg}	8	Laboratory test in HYPROP device and then fit the measurements to the Van Gnuthen model
HEAT	Volumetric heat capacity of grain particles, $(\rho c)_s$		1.97 MJ/(m³K)	Calculated from: ρ_s = 2700 [kg/m³] for silica quartz c_s = 730 [J/kg K] (Hemingway, 1987)
	Volumetric heat capacity of fluid (water), $(\rho c)_f$		4.2 MJ/(m³K)	Implemented by the FEFLOW program for water
	Thermal conductivity of grain particles, λ_s		4 W/(mK)	2.7 to 4.3 W/mK; Calculated by Johansen (1975)
	Thermal conductivity of the fluid (water), λ_f		0.65 W/(mK)	Implemented by the FEFLOW program for water
	Longitudinal dispersivity of sand, β_l		0.01 m	Calibration of the numerical model
	Transverse dispersivity of sand, β_t		0.005 m	Calibration of the numerical model
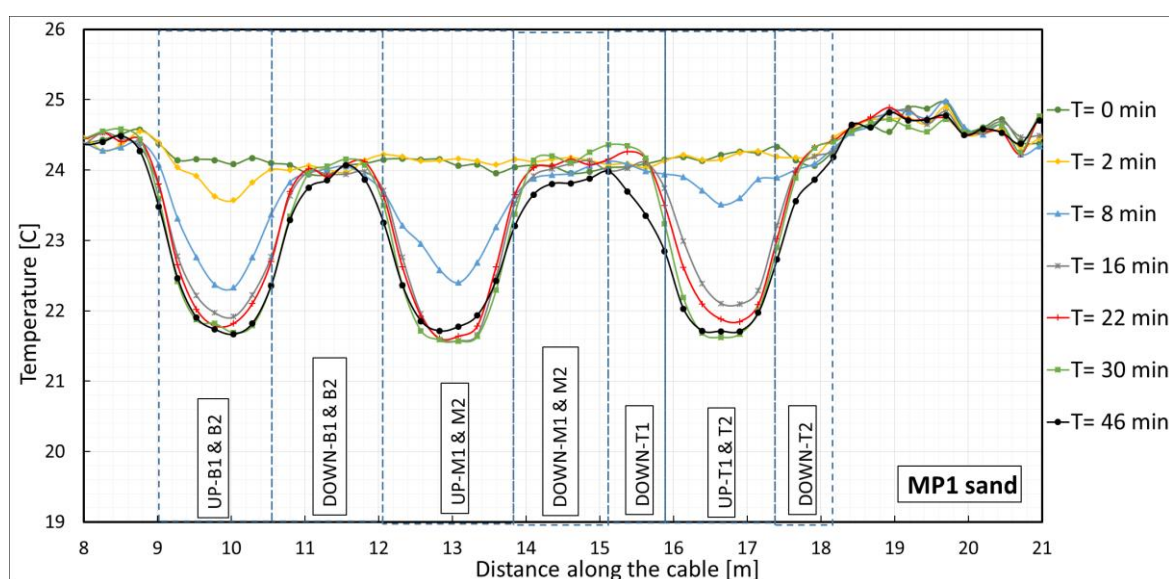
(a)
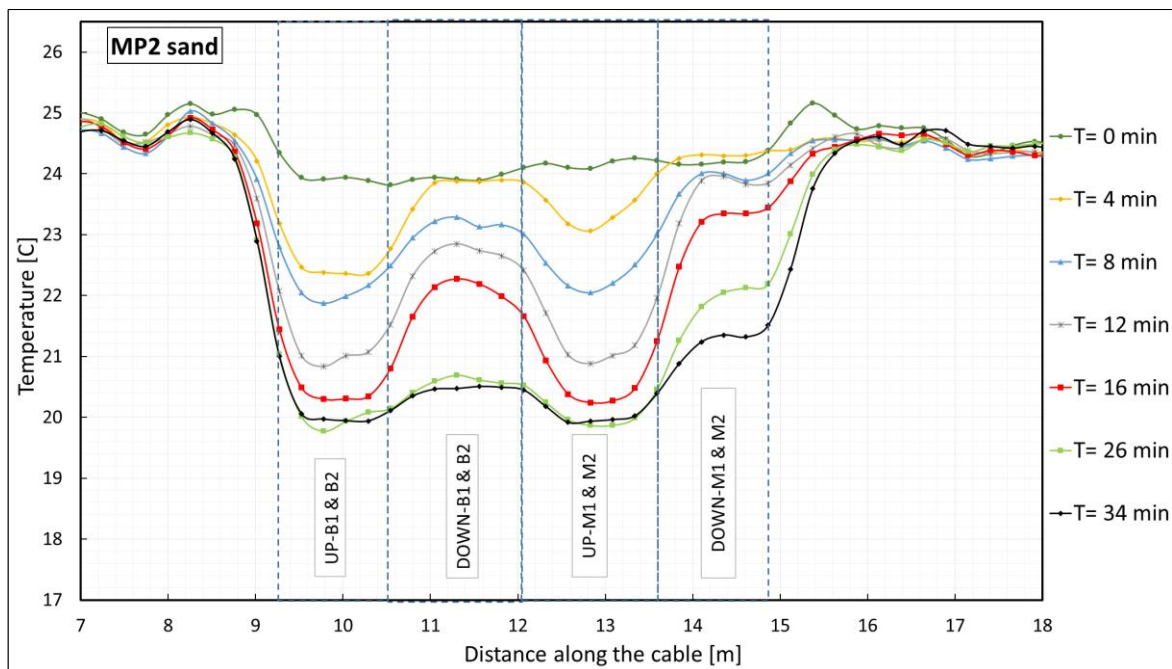
(b)
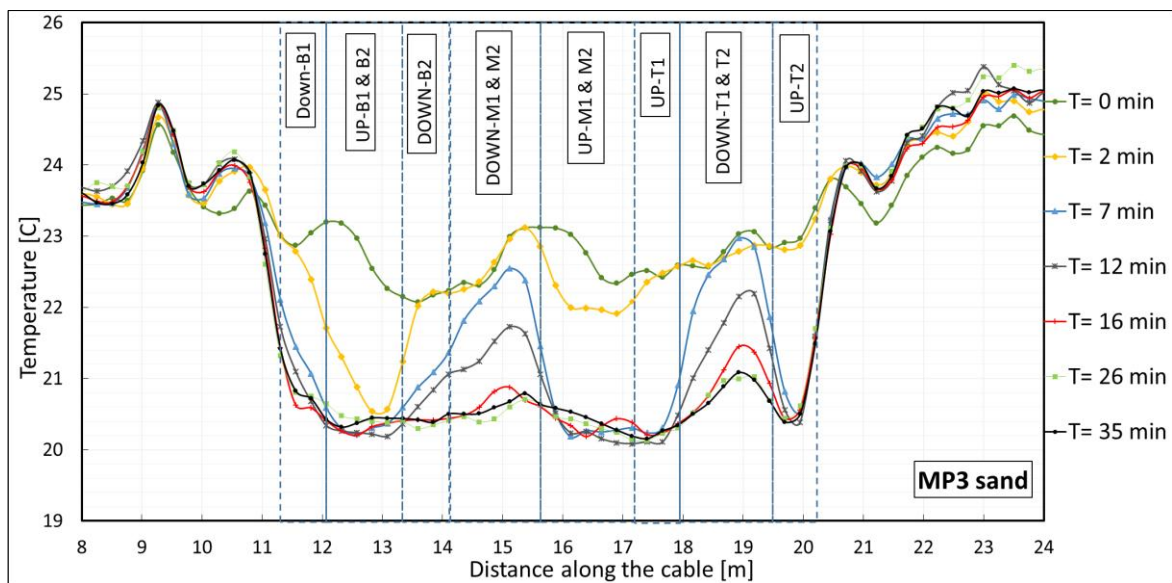
(c)

Figure 5: *Temperature measurement by the optical fiber DTS within the three types of silica sand during the laboratory experiment. (a) MP1 sand; (b) MP2 sand; (c) MP3 sand.*

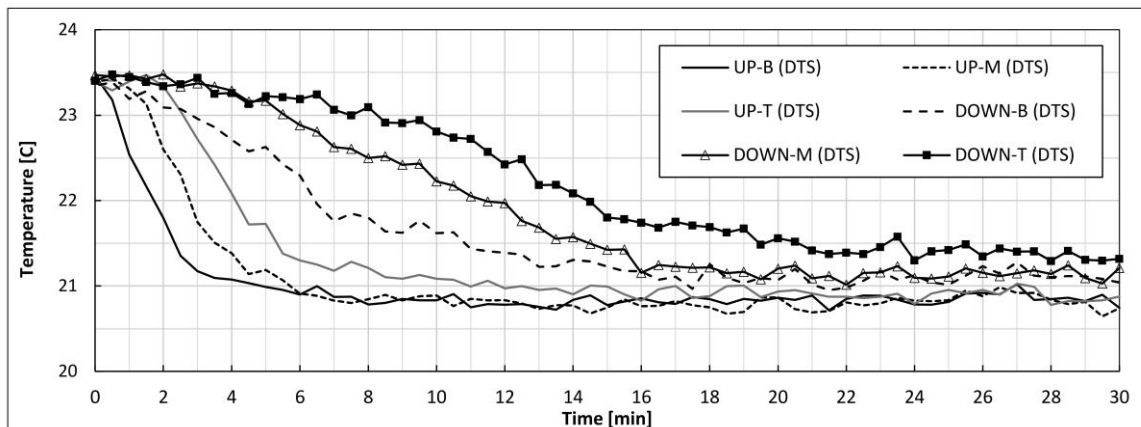***Slika 5:*** *Merjenje temperature z optičnimi vlakni v laboratoriju pri treh vrstah kremenčevega peska: (a) MP1; (b) MP2; (c) MP3.*

Figure 6: *Temperature variation in six measuring points within MP3 sand obtained by the optical fiber DTS.*

Slika 6: *Temperaturne razlike v šestih merilnih točkah v vzorcu MP3, izmerjene z optičnim kablom DTS.*
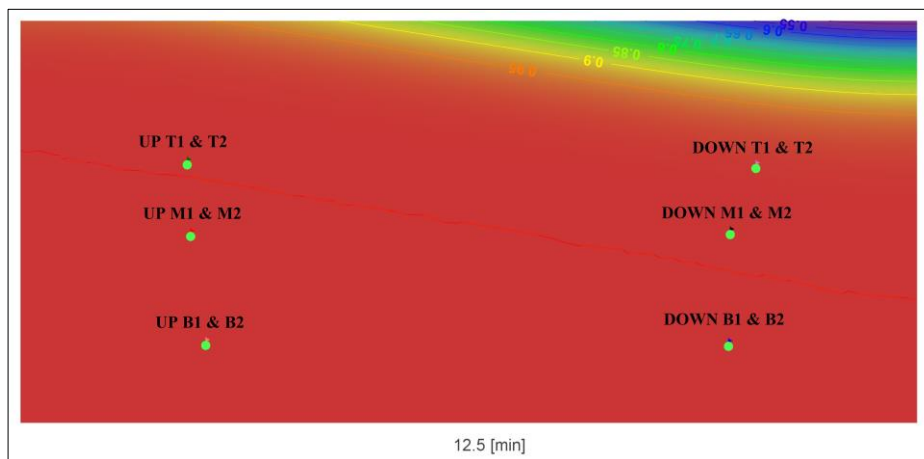

Figure 7: *Schematic results of saturation (%) for time T=12.5 min obtained from numerical modeling of MP3 sand with the measured value of saturated hydraulic conductivity (1.23 10-3 m/s) and porosity (0.435).*

Slika 7: *Shematski prikaz rezultata nasičenja (%) v času T = 12,5 min, pridobljenim z numeričnim modeliranjem vzorca MP3 z izmerjenima vrednostma koeficienta prepustnosti (1,23 10-3 m/s) in poroznosti (0,435).*
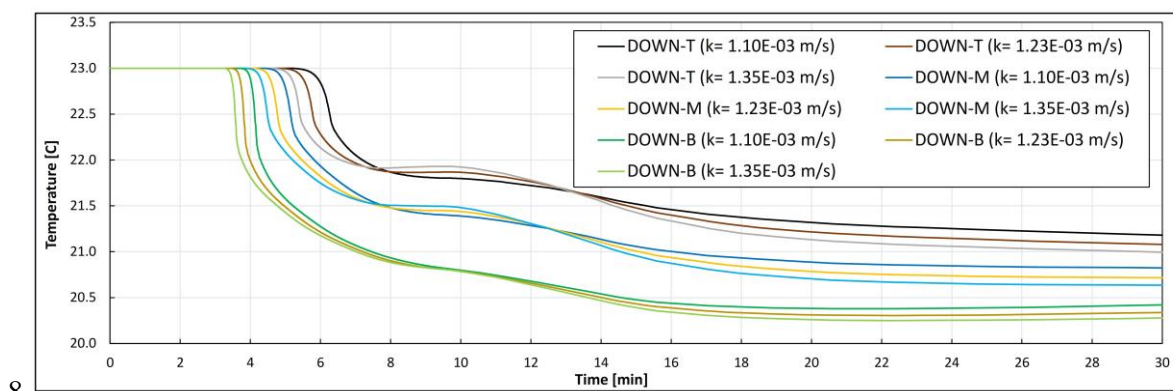
8

Figure 8: *Temperature results for the downstream measuring points obtained by the coupled hydrothermal numerical modeling of MP3 sand.*

Slika 8: *Rezultati povezanega hidravlično-termičnega numeričnega modela in meritev temperatur v merskih točkah na dolvodni strani za primer vzorca MP3.*

Ghafoori Y. et al.: Heat transfer by seepage in sand: Influence of saturated hydraulic conductivity and porosity – Vpliv koeficienta prepustnosti in poroznosti zemljin na prenos toplote s precejanjem

Acta hydrotechnica **34/60 (2021)**, 61–75, Ljubljana

By increasing the value of saturated hydraulic conductivity, the saturation front moves faster and the temperature drops sooner (see Figure 8) due to heat transfer by propagated water. A higher degree of saturation in measuring points increases the thermal velocity and the amount of heat transferred by convection that decreases the soil temperature to the temperature of water in the upstream tank. The flat section of the temperature lines (between 7 to 14 min) associates with a temporary decrease of water inflow and water table in the upstream tank during the experiment.

The influence of porosity was studied by numerical analysis considering four values for porosity within the range of ±5 percent of its measured value. Figure 9 shows the temperature results for measuring points located within the MP3 sand obtained from these numerical models.
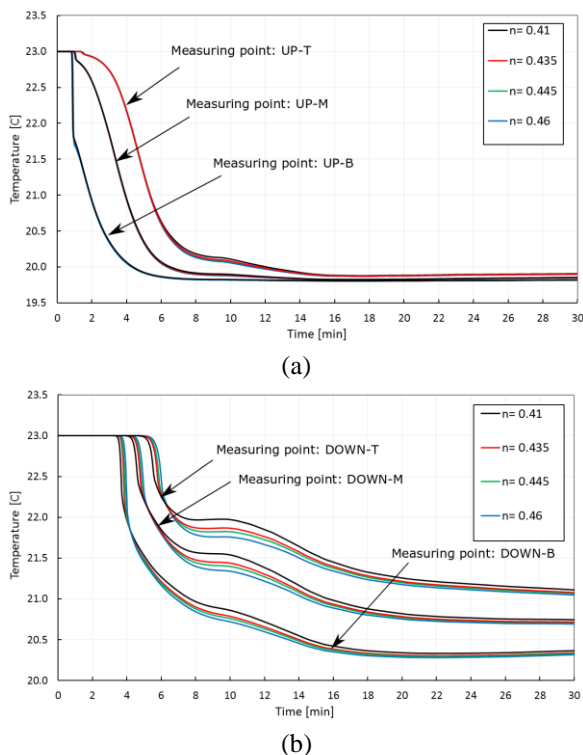

(a)

(b)

Figure 9: Temperature results of measuring points associate with numerical models with different values for porosity. (a) Measuring points adjacent to the upstream side; (b): Measuring points located model's downstream.

Slika 9: Rezultati numeričnega modeliranja z določitvijo temperature v merskih točkah za primer vzorca MP3 (a) merske točke gorvodno; (b) merske točke dolvodno.

Unlike the measuring points at the model's upstream section (see Fig 9a), the variation in the input value of porosity affects the temperature variation of the measuring points located in the downstream part (Fig 9b). For the sand with a higher porosity value, the temperature declination starts later but falls lower (See the blue line in Fig 9b), and it is inversely valid for the smaller porosity values (the black line in Fig 9b). This behavior can be described considering the equivalent heat capacity and thermal conductivity equations (Eq. 4 and Eq. 5), as well as the fluid pore velocity within the porous media.

By increasing the porosity, the overall volumetric heat capacity of sand in the saturated condition is increased, while the equivalent thermal conductivity is decreased. Also, with constant saturated hydraulic conductivity, slightly larger porosity decreases the velocity of the fluid in pores and consequently the speed of saturation front, wherefore temperature begins to decline later. When the pores are filled with water, the temperature decreases toward the water temperature.

In this paper, the temperature from the numerical simulation agreed better with the measured temperature by DTS compared to the coupled heat and seepage simulation performed in PLAXIS 2D by Ghafoori et al. (2020a). This can be due to the difference in the assignment of upstream thermal boundary. In FEFLOW a water temperature of 19.8 °C was assigned by the time-dependent function on the nodes of the upstream face, while in PLAXIS 2D a constant temperature equaling the water temperature was assigned for the upstream boundary. Also, the numerical model in FEFLOW was calibrated for heat dispersivity, which led to a better thermal simulation.

It should be mentioned that in a real-sized structure, the material anisotropy, variabilities in thermal and flow properties, fluid density variability, and complexity of the structure and boundary conditions should be considered. The site material's thermal properties in the site can be estimated with the help of geological maps, appropriate material sampling, and laboratory measurements of the samples (Janža et al., 2017).

The accuracy of temperature measurement by DTS strongly depends on the optical cable distribution as well as the calibration of the measurement.

Continuous measurement of temperature together with the coupled hydrothermal simulation can be used within the embankment and earthfill dams to detect the seepage flow or possible internal erosion. FEFLOW is an appropriate program to simulate the flow, mass, and heat transport within complex geometry and in the variably saturated medium. The program was already used for large-scale modeling of the groundwater flow in aquifers for the Soča River and Ljubljansko Polje basins in Slovenia (Vižintin et al., 2018; Vrzel et al., 2019).

This paper also presented the influence of saturated hydraulic conductivity and porosity in process of heat transfer by seepage flow in soil. Small variations in the value of these parameters will affect the thermal behavior of the soil subjected to seepage.

5. Conclusion

The coupled hydrothermal analysis of porous media subjected to seepage flow is a complex process that depends on both the material's thermal and hydraulic properties. The following conclusions are obtained from the experimental and numerical studies conducted in this paper:

- The thermal velocity is higher in the sand with higher hydraulic conductivity. This is because of the fast-moving of saturation front and due to the convection of heat by propagated water. In higher hydraulic conductivity sand, the temperature declination occurs earlier, and it is dropped down close to the temperature of water in the upstream tank.

- In MP1 sand with lower hydraulic conductivity, the influence of the capillary rise in heat transfer is remarkable.

- By increasing the sand's porosity, its volumetric heat capacity in the saturated

condition is increased while the overall thermal conductivity is decreased. Therefore, the temperature at the measuring point begins dropping later than at the sand with smaller porosity, but it drops down to the temperature of water in the upstream tank more quickly.

- For further study, it is proposed that a comprehensive sensitivity analysis be conducted to determine the influence of each thermal and hydraulic property of the material on the heat transfer process.

Acknowledgment

References

Bear, J., Verruijt, A. (1987). Modeling Groundwater Flow and Pollution. D. Reidel Publishing Company, Dordrecht, Holland. https://doi.org/10.1007/978-94-009-3379-8.

Brinkgreve, R.B.J., Kumarswamy, S., Haxaire, A. (2017). Thermal and coupled THM analysis. Plaxis bv, DELFT, Netherlands.

Bui, Q.C., Zhou, Y., Zhao, C., Nguyen, C.T. (2019) Numerical and Experimental Study of Coupled Seepage and Heat Transfer in Soil Medium. *Geotech. Geol. Eng.* **37**, 4981–4994. https://doi.org/doi.org/10.1007/s10706-019-00957-3.

Diersch, H.-J.G. (2014) FEFLOW: Finite Element Modeling of Flow, Mass and Heat Transport in Porous and Fractured Media. Springer. https://doi.org/10.1007/978-3-642-38739-5.

Dornstadter, J. (1997). Detection of internal erosion in embankment dams, in: Nineteenth International

Congress on Large Dams. International Commission on Large Dams, Paris, Florence, pp. 87–102.

Dornstädter, J., Heinemann, B. (2012). Temperature as Tracer for In Situ Detection of Internal Erosion Key words, in: 6th International Conference on Scour and Erosion. pp. 1369–1375.

Ghafoori, Y., Maček, M., Vidmar, A., Říha, J., Kryžanowski, A. (2020a). Analysis of seepage in a laboratory scaled model using passive optical fiber distributed temperature sensor. *Water* **12**. https://doi.org/10.3390/w12020367.

Ghafoori, Y., Maček, M., Vidmar, A., Říha, J., Kryžanowski, A. (2020b). Monitoring of temperature distribution by optical fiber DTS within soil subjected to seepage flow, in: Second SLOCOLD -MACOLD Symposium on Topic Water Reservoirs - an Active Measure in Adapting to Climate Change. Slovenian Committee on Large Dams, Macedonian Committee on Large Dams, Skopje, Republic of N. Macedonia and Ljubljana, Republic of Slovenia, pp. 77–84.

Ghafoori, Y., Vidmar, A., Říha, J., Kryžanowski, A. (2020c). A review of measurement calibration and interpretation for seepage monitoring by optical fiber distributed temperature sensors. *Sensors* **20**, 1–23. https://doi.org/10.3390/s20195696.

Hala, M., Petrula, L., Alhasan, Z. (2020). Comparison of hydraulic conductivity values obtained from empirical formulae and laboratory experiments. *Acta Univ. Agric. Silvic. Mendelianae Brun.* **68**, 669–678. https://doi.org/10.11118/actaun20206804669.

Hemingway, B.S. (1987) Quartz; heat capacities from 340 to 1000 K and revised values for the thermodynamic properties. *Am. Mineral*. **72**, 273–279.

Janža, M., Lapanje, A., Šram, D., Rajver, D., Novak, M. (2017) Research of the geological and geothermal conditions for the assessment of the shallow geothermal potential in the area of Ljubljana, Slovenia. *Geologija* **60**, 309–327. https://doi.org/doi.org/10.5474/geologija.2017.022.

Johansen, O. (1975) Thermal conductivity of soils. Ph.D. thesis. University of Trondheim, Trondheim, Norway.

Johansson, S. (1997) Seepage Monitoring in Embankment Dams. Doctoral Thesis. Royal Institute of Technology, Stockholm, Sweden.

Kaviany, M. (1991). Principles of Heat Transfer in Porous Media. Springer-Verlag, New York, USA. https://doi.org/10.1007/978-1-4684-0412-8.

Kema (2020). Filter kremenov pesek – beli vlažen [WWW Document]. URL http://www.kema.si/product/filter-kremenov-pesek-beli-vlazen/.

Liu, S., Masliyah, J.H. (2005). Dispersion in Porous Media, in: Vafai, K. (Ed.), Handbook of Porous Media. Taylor & Francis, FL, USA, pp. 81–140. https://doi.org/doi.org/10.1201/b18614.

Mars, J.I., Buchoud, E., Vrabie, V.D., Khan, A.A., Blairon, S., D'Urso, G. (2013). Source separation and distributed sensing: The key for an efficient monitoring, in: 2013 5th IEEE International Workshop on Computational Advances in Multi-Sensor Adaptive Processing, CAMSAP 2013. pp. 264–267. https://doi.org/10.1109/CAMSAP.2013.6714058.

Mohseni Languri, E., Domairrry Ganji, D. (2011). Heat Transfer in Porous Media, in: Heat Transfer - Mathematical Modelling, Numerical Methods and Information Technology. https://doi.org/10.5772/16210.

Nagy, L., Takács, A., Huszák, T., Mahler, A., Varga, G. (2013). Comparison of permeability testing methods, in: 18th International Conference on Soil Mechanics and Geotechnical Engineering. Paris, France, pp. 399–402.

Nield, D.A., Bejan, A. (2006). Convection in Porous Media. Springer, New York, USA.

Perzlmaier, S., Aufleger, M., Dornstädter, J. (2007). Detection of Internal Erosion by Means of the Active Temperature Method, in: Assessment of the Risk of Internal Erosion of Water Retaining Structures : Dams, Dykes and Levees. Intermediate Report of the European Working Group of ICOLD. Deutsches Talsperren Komitee.

Rubin, H. (1974). Heat dispersion effect on thermal convection in a porous medium layer. *J. Hydrol.* **21**, 173–185. https://doi.org/doi.org/10.1016/0022-1694(74)90035-3.

Schindler, U., Müller, L. (2017). Soil hydraulic functions of international soils measured with the Extended Evaporation Method (EEM) and the HYPROP device. *Open Data J. Agric. Res*. **3**, 10–16. https://doi.org/dx.doi.org/10.4228/ZALF.2003.273.

Silixa Ltd (2014). SILIXA XT-DTS Software Manual.

Sjödahl, P., Dahlin, T., Johansson, S. (2009). Embankment dam seepage evaluation from resistivity monitoring data. *Near Surf. Geophys*. **7**, 463–474. https://doi.org/10.3997/2214-4609.20146268.

Termit (2018). Catalog for Quartz and ceramic coated sands [WWW Document]. URL https://www.termit.si/en/wp-content/uploads/sites/3/2018/08/kremenov_pesek.pdf.

Van Genuchten, M.T. (1980). A Closed-form Equation for Predicting the Hydraulic Conductivity of Unsaturated Soils. *Soil Sci. Soc. Am. J.* https://doi.org/10.2136/sssaj1980.03615995004400050002x.

Vižintin, G., Ravbar, N., Janež, J., Koren, E., Janež, N., Zini, L., Treu, F., Petrič, M. (2018). Integration of models of various types of aquifers for water quality management in the transboundary area of the Soča/Isonzo river basin (Slovenia/Italy). *Sci. Total Environ.* **619–620**, 1214–1225. https://doi.org/10.1016/j.scitotenv.2017.11.017.

Vrzel, J., Ludwig, R., Vižintin, G., Ogrinc, N. (2019). An integrated approach for studying the hydrology of the Ljubljansko polje aquifer in Slovenia and its simulation. *Water* **11**. https://doi.org/10.3390/w11091753.